

# Decision-Making and Planning Method for Autonomous Vehicles Based on Motivation and Risk Assessment

Yisong Wang , Chunyan Wang , Wanzhong Zhao, and Can Xu

**Abstract**—In order to improve the real-time and computational efficiency of autonomous vehicles’ decision-making process, this paper draws on the decision-making behavior of human drivers with the motivation as the core and proposes a decision-making and planning method based on motivation and risk assessment. On the one hand, it analyzes and determines the motivations that cause the driving state to change for decision-making and planning. On the other hand, on the basis of the lateral trajectory prediction of surrounding vehicles, the longitudinal trajectory propensity prediction of different drivers is added to construct a risk assessment model that can reflect risk of the future time domain. Based on this, the motivation-based decision method is mapped into the risk assessment model, and a cost function is established to decouple the path and speed, so that the geometry and speed can be flexibly adjusted according to environmental risks. The simulation results show that the proposed method can effectively make driving behavior decisions and plan the trajectory in real time according to the current environment, which can improve the computational efficiency of the decision-making process and guarantee the safety at the same time.

**Index Terms**—Autonomous vehicle, decision-making, decouple planning, motivation, risk assessment.

## I. INTRODUCTION

WITH the rapid development of computer and communication technology, autonomous vehicles are getting more and more attention. Many automobile companies are committed to developing higher-level technologies for autonomous driving. In order to cope with different scenarios, advanced assistive technology and decision algorithm such as BSD, CTA, IACC are developed one after another. The behavior decision-making and planning facing various traffic environments and emergency situations is the core technology to ensure security and driving efficient of vehicles. However, it is still a challenge

Manuscript received May 22, 2020; revised October 29, 2020; accepted December 31, 2020. Date of publication January 8, 2021; date of current version February 12, 2021. This work was supported in part by the Industrial Technology Innovation Project of Anhui New Energy Vehicle and Intelligent Network Vehicle in 2019, in part by the National Natural Science Foundation of China under Grants 52072175 and 51875279, and in part by the Foundation of Graduate Innovation Center in NUAA (kjj20200201). The review of this article was coordinated by Dr. E. Velenis. (*Corresponding author: Chunyan Wang.*)

The authors are with the Department of Vehicle Engineering, Nanjing University of Aeronautics and Astronautics, Nanjing 210016, China (e-mail: wys2020@nuaa.edu.cn; wcy2000@126.com; zhaowz2020@126.com; xucan@126.com).

Digital Object Identifier 10.1109/TVT.2021.3049794

for autonomous vehicles to make accurate, efficient, and safe decision-making and planning in complex environments.

The decision-making and planning of the autonomous vehicle plans the local trajectory according to the specific road conditions, traffic rules, surrounding environmental conditions and so on. There are two main methods on behavioral decision-making and planning, that is, the rule-based method and the machine learning based method. The rule-based behavior decision-making method divides the behavior of autonomous vehicles, and establishes a behavior rule library according to driving rules, knowledge, experience, traffic rules, etc. [1], [2]. Then, the vehicle states are converted by logic rules and corresponding driving behaviors. Zhao etc. proposed a fast decision making system that accesses to the ontology-based knowledge base, which avoids collisions by following right-of-way traffic rules [3].

With the development of artificial intelligence, decision-making methods based on machine learning have received widespread attention. This method learns autonomously through environmental samples, and then establishes behavior rules by using self-learning data through different learning methods or network structures. Then, it outputs the decision behavior based on environmental information. The machine learning method mainly includes deep learning method (DNN), reinforcement learning (RL) method, recurrent neural network (RNN), etc. [4]–[9]. DNN has great flexibility in modeling realistic problems. The end-to-end decision-making method based on DNN network can directly sense the input image from the environment and output decision behavior to the control actuator [10]. RL is very popular nowadays due to their performance in the field of artificial intelligence. David etc. used the deep Q-networks to learn and explore intersections, which can solve the problem of collision avoidance under occluded cars [11]. Meanwhile, the method of using a multi-criteria cost function to filter multiple alternatives generated in the current environment is also adopted [12], [13]. In addition, the concept of potential field is also used in decision-making and planning [14], [15]. Khajepour etc. used a three-dimensional virtual dangerous potential field which divides the surrounding vehicles and target points into repulsive and gravitational fields to select the best trajectory [16]. Nowadays, decision and planning methods mostly rely on value-based decision models [17], [18], and mainly use probabilistic road map (PRM) and rapid-exploration random tree (RRT) method [19]. Alesiani proposed a heuristic explored tree

algorithm for motion planning that locally growing a random tree to find the optimal trajectory [20]. By sampling the continuous state space, these methods generate all possible alternative paths and select the most suitable driving route through the optimal utility theory. However, these methods require a global search, that is, each possible arrival position and candidate trajectory are screened within each decision step. In the actual cases, human drivers do not plan all feasible trajectories in their mind every moment. Therefore, the existing methods have low calculation efficiency, and is difficult to ensure the real-time requirements of autonomous vehicles during driving. What's more, the commonly used quintic polynomial planning method can plan a smooth trajectory with quadratic derivation. However, it rarely considers the speed distribution of each node resulting in the trajectory shape often fixed [21]. Therefore, it is difficult to properly adjust its geometry according to the surrounding environment and has poor flexibility.

To address the above issues, this work analyzes the surrounding environmental conditions and motivations when the vehicle may change the state under the highway environment, and then a decision-making and planning method for autonomous vehicles based on motivation and risk assessment is proposed. The main contributions of this work is listed as follows.

1) Proposing a decision mechanism based on motivation trigger and using risk assessment model to verify the feasibility of decision results, so as to avoid meaningless decision, improve computational efficiency and ensure safety.

2) Considering the driving propensity prediction and lateral prediction of surrounding vehicles, and then a risk assessment model that can reflect the future time domain is constructed to realize the accurate prediction and assessment.

3) Decoupling the path and speed by Frenet coordinate so that the path geometry and the speed distribution can be adjusted according to the surrounding risks, which is more realistic and flexible in planning.

The rest of this paper is organized as follows: Section II builds the behavior prediction model and risk assessment model of surrounding vehicles. Section III introduces the decision and planning method, where Section III-A extracts, analyzes, and models the motivations that cause the vehicle's driving state to change under the highway environment. Section III-B maps the results of the motivation model to the risk assessment model for dynamic environment verification, and then gets the optimal target point. In Section III-C, the path and speed of the autonomous vehicle is planned flexibly. Finally, simulations result and corresponding discussions are included in Section IV to show the workings of the proposed method. Conclusions are offered in Section V.

## II. BEHAVIOR PREDICTION AND RISK ASSESSMENT MODELS

The decision-making process not only needs to consider the ego vehicle's situation, but also needs to consider its interaction with surrounding vehicles [22]. Predicting the movement of surrounding vehicles can predict the dynamic changes of the traffic environment in the future, and it is a necessary premise for autonomous vehicles to make behavioral decisions and

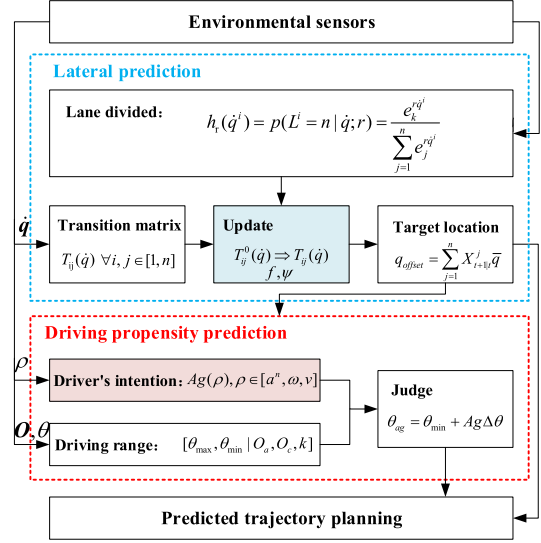


Fig. 1. The structure of behavior prediction model.

trajectory planning. Therefore, this section gives the behavior prediction model of the surrounding vehicles, integrates the behavior prediction results of the object vehicles, and uses the time to collision (TTC) and the time headway (Th) to construct the risk assessment model that can reflect the traffic environment in the future.

### A. Behavior Prediction Model

In actual traffic scenarios, surrounding vehicles' future behaviors are the main source of uncertainty in motion prediction. Meanwhile, the interaction between vehicles also add great challenges for the prediction. Current behavior prediction models include recurrent neural networks (RNN), interacting multiple model (IMM), or machine learning methods, etc. As shown in Fig. 1, The behavior prediction model proposed in this paper mainly includes two parts: 1) lateral prediction of surrounding vehicles; 2) driving propensity prediction. It simplifies the prediction of lateral behavior to the choice of target lane. By calculating the probability of each lane sequence, the lane order which the vehicle is most likely to choose is selected. As the surrounding vehicle's longitudinal driving trajectory also have an impact on the vehicle driving in its target lane, this paper adds the driver's tendency prediction in the driving direction of the vehicle on the basis of the lateral prediction.

1) *Lateral Prediction:* Behavior prediction can be expressed as the probability of predicting the vehicle's transition from the current state to another state. This relationship of state transition can be described as a Markov chain, where the probability of transition between states is determined by the Markov transition probability matrix (MTPM). Predicting the transition of the state between the lateral behavior of the vehicle can be understood as the choice of the lane, that is, the vehicle changes from the lane  $i$  to the lane  $j$ ,  $|i - j| = 0$  means lane keeping;  $|i - j| = 1$  means lane changing;  $|i - j| = 2$  means double lane changing. The lateral speed of the vehicle corresponding to each behavior is different, so the behavior of the predicted vehicle is classified

according to the lateral speed. The SoftMax regression strategy can map the target to a probability distribution for classification. Therefore, this work adopts the SoftMax regression strategy to change the lane selection problem into a multi-classification problem based on the lateral speed range.

The execution process of the behavior prediction model is as follows: for moment  $t$ , The state relationship of the predicted vehicle in each lane is a Markov chain, and its state sequence can be expressed as:

$$\begin{cases} S_t = \{\dot{q}_t^1, q_t^1, P_t^1; \dot{q}_t^2, q_t^2, P_t^2; \dots \dot{q}_t^n, q_t^n, P_t^n\} \\ \sum_i^n P_t^i = 1 \end{cases} \quad (1)$$

where  $n$  is the lanes number;  $q_t^i$  is lateral offset;  $\dot{q}_t^i$  is the lateral speed;  $P_t^i$  is the probability of the predicted vehicle in the lane  $i$ .

When the state of the predicted vehicle at moment  $t$  is determined, the state at  $t+1$  is completely determined by the state transition matrix. In the lateral behavior of the vehicle, the lateral speed plays a vital role. The state transition matrix based on the lateral speed is as follows:

$$T_{ij}(\dot{q}) = \begin{bmatrix} T_{11} & T_{12} & T_{13} \\ T_{21} & T_{22} & T_{23} \\ T_{31} & T_{32} & T_{33} \end{bmatrix} \quad (2)$$

where  $T_{ij}$  is the probability that the predicted vehicle change from lane  $i$  to lane  $j$ .

$$T_{ij} = P(L_{t+1} = j | L_t = i) \quad (3)$$

The lateral velocity-dependent transition probability is calculated as follows, firstly, the multi-lane classification model is constructed:

$$h_r(\dot{q}^i) = \begin{bmatrix} p(L^i = 1 | \dot{q}; r) \\ p(L^i = 2 | \dot{q}; r) \\ \vdots \\ p(L^i = n | \dot{q}; r) \end{bmatrix} = \frac{1}{\sum_{j=1}^n e^{r\dot{q}^i}} \begin{bmatrix} e_1^{r\dot{q}^i} \\ e_2^{r\dot{q}^i} \\ \vdots \\ e_n^{r\dot{q}^i} \end{bmatrix} \quad (4)$$

where  $r$  is the parameter of the model;  $L^i = n$  is the lane numbers.

The input is converted into an exponential form so that the larger one becomes greater, and the probability of being selected will become larger. In this way, the probability distribution can be reflected more clearly. Replace exponent  $e$  with Gaussian probability density function (PDF) and Gaussian cumulative function (CDF) based on lateral velocity  $\dot{q}$ .

$$\begin{cases} f(\dot{q}, \mu, \sigma) = \frac{1}{\sigma\sqrt{2\pi}} e^{-\frac{(\dot{q}-\mu)^2}{2\sigma^2}} \\ F(\dot{q}, \mu, \sigma) = \frac{1}{\sigma\sqrt{2\pi}} \int_{-\infty}^{\dot{q}} e^{-\frac{(q-\mu)^2}{2\sigma^2}} dq \end{cases} \quad (5)$$

After obtaining the classification model and the state transition matrix, the state transition matrix is updated and calculated as shown in Fig. 2. The Gaussian distribution of different lateral behaviors of vehicles is extracted from the NGSIM database and made improvements to adapt to the transitional relationship between the two behavior accurately. Furthermore, the state transition matrix can be updated by the lateral offset and speed

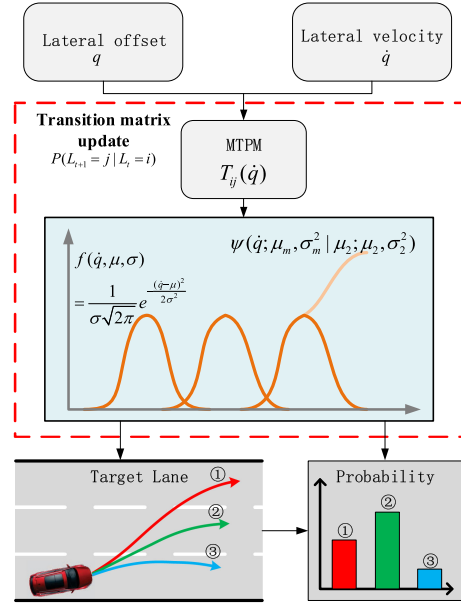


Fig. 2. The update process of MTPM.

of the vehicle, and the probability of different behaviors can be output.

When the Gaussian distribution is used to update the state transition, both the PDF and the CDF cannot fully adapt to the expression of vehicle state based on lateral velocity, which is likely to lead to the prediction inaccurately. Therefore, in this paper, the PDF based on lateral velocity is improved. On the right side of the Gaussian distribution center corresponding to the double lane change, a function  $\psi(\dot{q}; \mu_m, \sigma_m^2 | \mu_2; \sigma_2^2)$  is used to make the distribution value similar to the form of the CDF in Fig. 2. When the state is  $\dot{q} > \mu_2$  and  $|i - j| == 2$ , this makes up for the problem that the PDF shows a downward trend as  $\dot{q}$  continues to increase. In this condition, the updated value of the MTPM tending to double lane change should be continuously increasing. Meanwhile, the advantage of the Gaussian distribution for the smooth transition between the two behaviors is also retained. The update calculation of MTPM is as follows:

$$T_{ij}^0(\dot{q}) = \begin{cases} T_{ij}^{ini} + f(\dot{q}; \mu_m, \sigma_m^2) \\ T_{ij}^{ini} + \psi(\dot{q}; \mu_m, \sigma_m^2 | \mu_2; \sigma_2^2) \end{cases} \quad (6)$$

$$f(\dot{q}; \mu_m, \sigma_m^2) = \begin{cases} f(\dot{q}; \mu_0, \sigma_0^2), |i - j| = 0 \\ f(\dot{q}; \mu_1, \sigma_1^2), |i - j| = 1 \\ f(\dot{q}; \mu_2, \sigma_2^2), |i - j| = 2 \end{cases} \quad (7)$$

$$T_{ij}(\dot{q}) = \frac{T_{ij}^0(\dot{q})}{\sum_{j=1}^n T_{ij}^0(\dot{q})} \quad (8)$$

where  $T_{ij}^{ini}$  is the initial state transition matrix;  $\mu_m$  and  $\sigma_m^2$  are the mean and variance of PDF;  $m$  is the number of driving behaviors;

The specific form of the function  $\psi(\dot{q}; \mu_m, \sigma_m^2 | \mu_2; \sigma_2^2)$  is as follows:

$$\psi(\dot{q}; \mu_m, \sigma_m^2 | \mu_2; \sigma_2^2) = 2f(\mu_2; \mu_2, \sigma_2^2) - f(\dot{q}; \mu_m, \sigma_m^2) \quad (9)$$

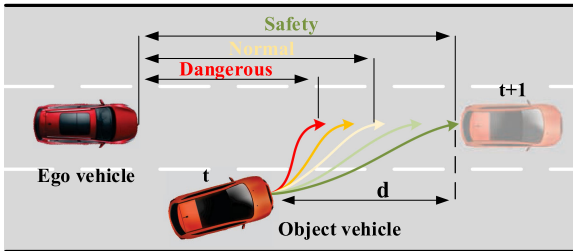


Fig. 3. The influence of different longitudinal trajectory trends.

TABLE I  
FUZZY LOGIC RULES

Parameter	VS	S	M	H	PH
S	C	C	N	A	A
M	C	C	N	A	A
H	N	N	A	A	A

The probability sequence that the predicted vehicle changes from lane  $i$  to lane  $j$  is:

$$X_{t+1|t}^j = P_{ij}(\dot{q})X_t^i \quad (10)$$

After obtaining the transition probability between lanes, the lateral position of the predicted vehicle at the next moment can be calculated by (11).

$$q_{offset} = E(X_t^i) = \sum_{j=1}^n X_{t+1|t}^j \bar{q} \quad (11)$$

2) *Driving Propensity Prediction*: Previous section gives the predicted lateral position. However, considering the different personalities of the driver or the influence of the surrounding environmental factors, the longitudinal displacement will also be different under the same lateral position [23], [24]. Fig. 3 is the influence of different longitudinal trajectory trends. It can be seen from Fig. 3 that different longitudinal trajectories of object vehicle have significantly different risks for ego vehicle, which directly affects the decision-making behavior of ego vehicle at the next moment.

Predicting the trajectory of surrounding vehicles is not a deterministic task, it depends on the driving habits of each driver. However, the driver's intention cannot be directly judged, and the vehicle's dynamic parameters can only partially reflect its behavior. The logic between them is not directly a matter of yes or no. Therefore, this work uses fuzzy logic method to predict the driving style of different drivers. It helps to link the driver's intention with the vehicle's characteristic signal, and provides an appropriate way to express the uncertainty of driving behavior.

In this work, the aggressiveness is used to indicate the driver's tendency of trajectory. The lateral acceleration  $a_n$  and yaw rate  $\omega$  that have a greater influence on the lane change path are selected as inputs of fuzzy logic, and then output the aggressiveness value. Fuzzy logic rules is constructed as shown in Table I. The yaw rate is blurred into linguistic variables "very small" (VS), "small" (S), "medium" (M), "large" (H), "large" (PH). The acceleration is blurred into linguistic variables "small" (S), "medium" (M), and "large" (H). Finally, it outputs the

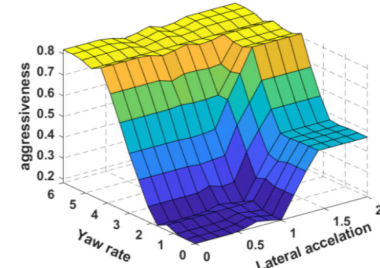


Fig. 4. The influence of lateral acceleration and yaw velocity on driving aggressiveness.

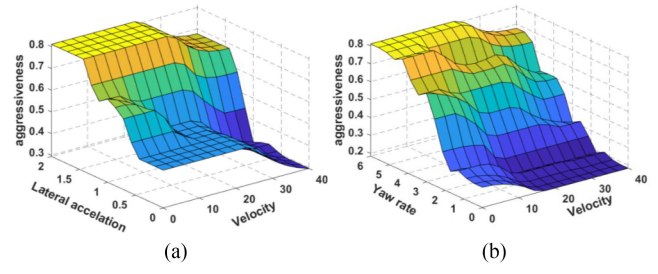


Fig. 5. The dampening effect of speed on driving aggressiveness. (a) The influence of lateral acceleration and velocity on driving aggressiveness. (b) The influence of yaw velocity and velocity on driving aggressiveness.

driver's aggressive progress as "aggressive" (A), "normal" (N), "conservative" (C).

Fig. 4 shows the influence of lateral acceleration and yaw velocity on driving aggressiveness. It can be seen from Fig. 4 that the aggressiveness increases continuously with the increase of lateral acceleration and yaw rate. In addition, speed also plays an important role in whether the trajectory is aggressive or not. However, compared with the first two factors, speed has a dampening effect on the aggressiveness. Fig. 5 shows the dampening effect of speed on driving aggressiveness. As shown in Fig. 5, with the increase of the speed, the aggressiveness is reduced, and the driver is more inclined to choose a smooth trajectory to ensure the stability of the vehicle.

The logic rules and the degree of membership are established for the input variable language, and the minimal implication method is adopted to calculate the degree of membership.

$$\chi_\rho = \min [\chi_a \ \chi_\omega \ \chi_v] \quad (12)$$

where  $\rho$  is the type of the input parameter.

The driving aggressiveness is obtained by using the center of gravity method to de-fuzzification.

$$Ag = \frac{\sum_u \chi_\rho^u w_\rho^u}{\sum_u \chi_\rho^u} \quad (13)$$

The result of driving aggressiveness is proportional to the yaw angle of each trajectory with different tendencies, so as to predict the corresponding trajectory according to the characteristics of the driver. According to the environment sensing module, the observed vehicle status is obtained, including the global coordinate position, vehicle speed, acceleration, yaw angle and

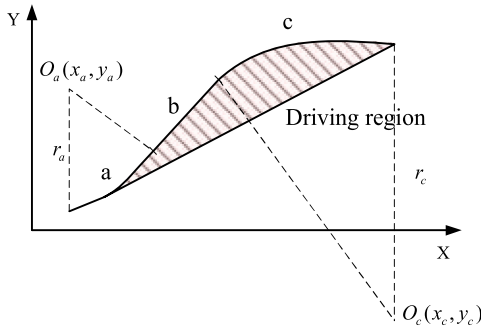


Fig. 6. The driving-region of lane changing process.

yaw angle velocity:

$$\boldsymbol{S}_{st} = [x_{st}, y_{st}, v_{st}, \theta_{st}, a_{st}, \omega_{st}]^T \quad (14)$$

The lane change process is divided into three parts, as shown in Fig. 6. Parts *a* and *c* are curve sections, and the vehicle approximates circular motion. Part *b* is a line tangent to the circle of part *a* and *c*. The curvature of part *a* is determined by the initial state of the vehicle, so the upper limit of the trajectory is determined by the curvature of part *c*. The smaller the curvature, the greater the slope of segment *b*, which means that the yaw angle of the vehicle is greater and the trajectory is more aggressive. When the trajectory is very smooth, the lower limit of the trajectory can be approximated as the connection of the initial and final states as shown in Fig. 6.

Based on Fig. 6, the maximum and minimum of yaw angle corresponding to the upper and lower limits of the trajectory is obtained:

$$v_a = \omega_a r_a \quad v_c = \omega_{\min} r_c \quad (15)$$

$$(s_x - x_c)^2 + (s_y - y_c)^2 = r_c^2 \quad (16)$$

where  $r_a$ ,  $r_c$  are the radius of the curve *a*, *c*;  $s_x$ ,  $s_y$  are the longitudinal and lateral displacement of the vehicle.

The calculation process of yaw angle related to different driving aggressiveness is as follows:

$$\begin{cases} d_1 = (y_a - kx_a - g)/\sqrt{(k^2 + 1)} = r_a \\ d_2 = (y_c - kx_c - g)/\sqrt{(k^2 + 1)} = r_c \end{cases} \quad (17)$$

where  $k, g$  are parameters of the straight-line segment of the trajectory.

$$\begin{cases} \theta_{\max} = \arctan(k) \\ \theta_{\min} = \arctan(\frac{s_y + r_c - r_a}{s_x - x_a}) \end{cases} \quad (18)$$

$$\theta_{ag} = \theta_{\min} + Ag\Delta\theta \quad (19)$$

3) *Quartic Polynomial Trajectory*: The predicted trajectory can be determined according to the initial state of the vehicle, predicted lateral position and yaw angle which are calculated in Section A and Section B. There are totally five constraints, so the quartic polynomial is adopted to fit the trajectory as:

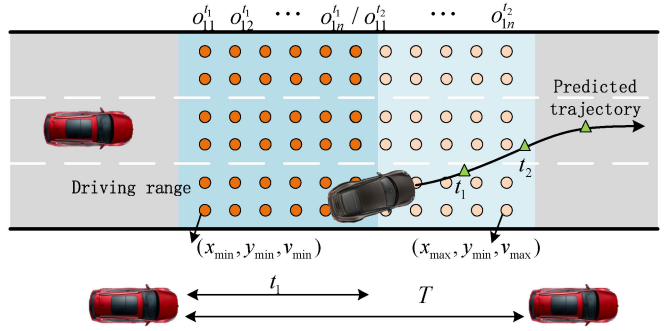


Fig. 7. The schematic diagram of risk assessment model.

$$y = a_0 + a_1 x + a_2 x^2 + a_3 x^3 + a_4 x^4 \quad (20)$$

$$\begin{cases} y(x_s) = y_s, \tan \theta_s = \frac{dy}{dx} \Big|_{(x_s, y_s)} \\ \tan \theta_{Ag} = \frac{dy}{dx} \Big|_{(x_m, y_m)} \\ y(x_d) = y_d, \tan \theta_d = 0 = \frac{dy}{dx} \Big|_{(x_d, y_d)} \end{cases} \quad (21)$$

where  $x_s, y_s, x_d, y_d$  are the initial and final position of the predicted vehicle;  $x_m, y_m$  are the position of the predicted vehicle when crossing the lane border.

### B. Risk Assessment Model

The changing traffic environment is the main factor affecting vehicle safety, so it is necessary to consider future environmental risks in the decision-making process. This section establishes a risk assessment model based on the prediction trajectory of each vehicle within the detectable range around the autonomous vehicle. Fig. 7 is the schematic diagram of the risk assessment model. The driving range of the autonomous vehicle is represented by a lattice, which is recorded as  $O(t)$ , and represented by a blue rectangle. Each dot in the lattice represents a status point of the autonomous vehicle. The predicted vehicle trajectory is also decomposed into position points related to the driving range of the autonomous vehicle at different times, represented by green triangles. By calculating the time-to-collision (TTC) and time headway (Th) between the predicted vehicle's position point and the state point in the lattice at each moment, the environment risk around the autonomous vehicle can be obtained. After getting the environmental risk, it provides the foundation for the decision and planning in the Section III.

In the driving range lattice  $O(t)$ ,  $x_e, y_e, v_e$  corresponding to each point  $o = (x_e, y_e, v_e)$  respectively represent the longitudinal position, lateral position and speed of the vehicle, and they are determined by the acceleration of the vehicle. Therefore, each state point can be expressed as:

$$\begin{cases} A_t = a_{e,\min} : \Delta a_e / C_p : a_{e,\max} \\ a_{e,k}^t = A_t(k) \\ v_{e,k}^t = a_{e,k}^t \cdot t \\ x_{e,k}^t = v_{e,k}^t \cdot t + \frac{1}{2} a_{e,k}^t \cdot t^2 \\ y_{e,k}^t = l_{\min} + (\Delta l / C_p)k \end{cases} \quad (22)$$

where  $a_{e,\min}$  and  $a_{e,\max}$  are the minimum and maximum acceleration limited by the autonomous vehicle;  $\Delta a_e = a_{e,\max} -$

$a_{e,\min}$ ;  $C_p$  is the number of vehicle speed and path candidates;  $l_{\min}$  is the lower boundary of the road.

Research shows that the driver's judgment of threat is mainly affected by two factors of Th and TTC [25]. Using the TTC indicator alone to quantify the level of danger often ignores the safety problems caused by the small distance when the speeds of the two vehicles are similar or even equal. However, Th is easy to underestimate the risk when the relative speed of the two vehicles is large. Therefore, TTC and Th are combined to build the risk assessment function in this paper.

$$\begin{cases} TTC = \frac{\varepsilon D(t)}{V_e(t) - V_f(t)} \\ Th = \frac{\varepsilon D(t) + L}{V_e(t)} \end{cases} \quad (23)$$

where  $D(t)$  Represents the distance between the autonomous vehicle and the preceding vehicle at time  $t$ ;  $V_e(t)$  and  $V_f(t)$  are the speed of autonomous vehicle and preceding vehicle;  $L$  is the length of the preceding vehicle;  $\varepsilon$  is the loss factor.

It's worth noting that both TTC and Th can only assess the risk for single-lane, while the actual driving needs to consider the vehicle merging on both sides. Therefore, this work uses loss factor  $\varepsilon$  to indicate the impact when the object vehicle and the autonomous vehicle belong to different lanes. When the two vehicles are in the same lane,  $\varepsilon = 1$ . In other cases,  $\varepsilon$  decreases with the increase of the lane distance. Then, the collision risk is calculated by the predicted trajectory sequence of each surrounding vehicle in the time domain  $T$  and the state set sequence of the autonomous vehicle.

$$\xi(z, T) = \frac{1}{z} \sum_k^z \sum_t^T \exp \left[ \gamma \left( \frac{\omega_{Th}}{Th_{k,t}} + \frac{\omega_{TTC}}{TTC_{k,t}} \right) \right] \quad (24)$$

where  $z$  is the number of vehicles in the detection range;  $\omega_{Th}$ ,  $\omega_{TTC}$  are the weight factors, respectively equal to 1 and 4;  $\gamma$  is the time loss factor. Obviously, the surrounding vehicle state information obtained at the current moment is the most accurate and has the greatest impact on the decision. As the forecast time increases, the uncertainty increases, and the impact on the initial decision will be smaller. Therefore,  $\gamma$  is a variable that decreases with time in a prediction time domain  $T$ .

### III. DECISION AND PLANNING METHOD BASED ON MOTIVATION AND RISK ASSESSMENT

In the decision-making process of autonomous vehicles, the local trajectory always changes with the dynamic traffic environment. The commonly used methods, such as PRM and RRT are to uniformly sample each point in the state space, then connect each sample point to build a set of travel trajectory candidates, and finally remove the collision trajectory. However, a human driver is not planned all feasible trajectories in every moment. Meanwhile, performing an optimal path selection at every moment has an impact on both computational efficiency and real-time. This work draws on the behavior of human drivers to make decision-making and planning for autonomous vehicles.

Fig. 8 shows the schematic diagram of decision-making and planning based on motivation and risk assessment. The decision-making process calculates the acceleration and lateral position

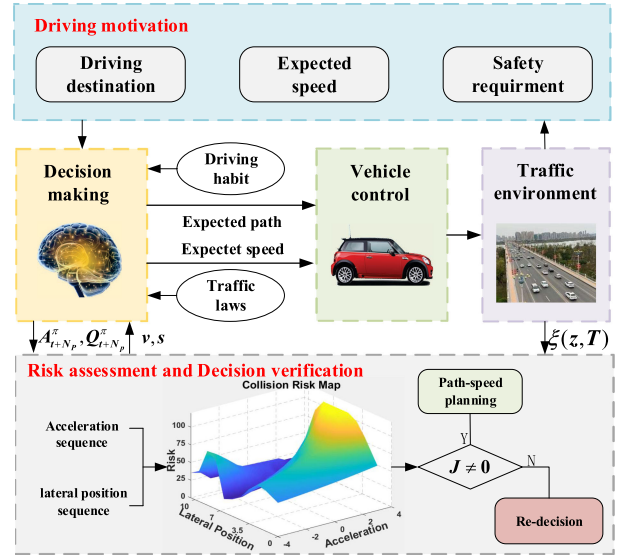


Fig. 8. Schematic diagram of decision-making and planning based on motivation and risk assessment.

candidate sequences  $(A_{t+N_P}^\pi, Q_{t+N_P}^\pi)$  according to different driving motivations and inputs them to the risk assessment module for safety verification. Then the evaluation function determines whether there is an optimal expected speed  $v$  and target lateral position  $s$  through the collision risk map. Finally, the result is passed back to the decision-making layer to control the vehicle and transfer  $\xi(z, T)$  after interacting with the traffic environment to the verification module in real time so that a complete closed-loop operation during the driving process of autonomous vehicles is realized. If all candidate sequences do not meet the safety requirements, the decision will be made again. In addition, in path-speed planning module, this work gets the candidate set of desired speed and lateral position of the vehicle through decision-making methods, and uses coordinate transformation to decouple the path and speed. Furthermore, it considers environmental risk factors to make them capable of adjustment.

#### A. The Decision Method Based on Motivation

In the process of driving, human drivers make reasonable decisions according to driving experience and traffic rules when the current state is not in line with the expected state or they perceive the occurrence of danger. With reference to human drivers, the motivation to change the vehicle state can be summarized as: 1) Expected speed; 2) Safety requirements; 3) Destination needs. In this paper, the decision-making process based on motivation is set as follows. When the motivation of changing state is generated, the decision is carried out according to different motivations. Otherwise, the vehicle stays in its current state to avoid frequent and meaningless decisions.

1) *Expected Speed*: The expected speed refers to the maximum safe speed that the driver thinks can be achieved in the current traffic environment. The difference between the expected and actual speeds is the main incentive for the vehicle to change its current state. In this paper, the radial basis function (RBF)

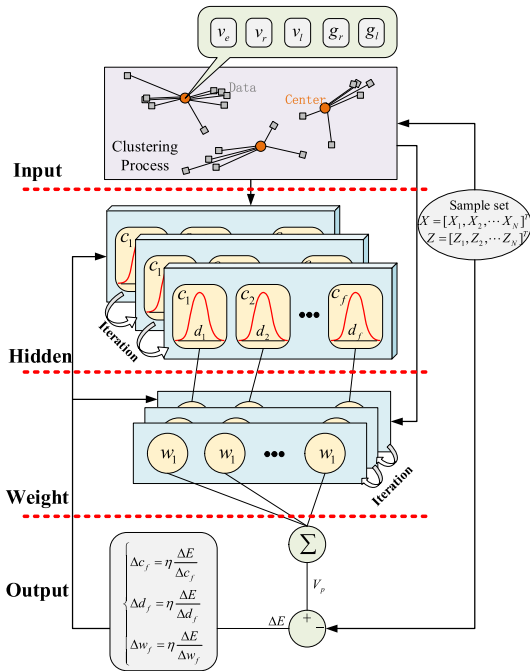


Fig. 9. The structure of RBF network.

neural network is used to simulate the decision-making process of drivers on the expected speed and make the decision-making behavior of autonomous vehicles more anthropomorphic.

RBF network can adjust the neuron center and width of each hidden layer according to the influence of input conditions on the output data, so that the output of a particular neuron is relatively large [26]. In this way, RBF can achieve local feedback and adjust the priority of input conditions. Fig. 9 shows the structure of RBF network. According to the prior knowledge obtained from NGSIM database, the vehicle speed \$v\_e\$, relative speed of preceding vehicle \$v\_r\$, the difference between vehicle speed and limit speed \$v\_l\$ and road space on both sides \$g\_l, g\_r\$ are selected as the input of RBF. Moreover, the K-means clustering algorithm is used to preprocess the input samples and determine the initial parameters of the hidden layer. The expected speed predicted by RBF network is expressed as follows:

$$V_p = \sum_{i=1}^f w_f \varphi_f(\|X - C_f\|) \quad (25)$$

where \$X = [v\_e \ v\_r \ v\_l \ g\_r \ g\_l]^T\$; \$C\_f\$ is the central parameter of each neuron in the hidden layer; \$f\$ is the number of neurons in the hidden layer; \$w\$ is the weight of the hidden layer to the output layer; \$\varphi\$ is the basis function;

$$\varphi_f = \exp \left( -\frac{\|X - C_f\|^2}{D_f^2} \right) \quad (26)$$

The RBF network basis function takes the distance \$\|X - C\_f\|\$ between the input vector and the threshold vector as the independent variable. In addition, in order to maximize the reflection of different input information by different hidden layer neurons, each center parameter of hidden neuron contains an expansion constant \$D\$. Therefore, it needs to reasonably determine center

parameters of hidden layer. This work uses the K-means clustering method to select the RBF center.

Clustering is an unsupervised learning, which groups similar objects into the same cluster. K-means clustering is an algorithm for finding clusters whose number is \$k\$ in a given data set. The size of \$k\$ is given by the user and can be calculated by the elbow method. The K-means clustering categorizes samples by calculating the Euclidean distance from all sample data to the \$k^{th}\$ central sample data.

$$d_{ij} = \|X_i - c_j\|^2 \quad (27)$$

$$K_j = \left\{ d_{ij} \leq \|X_i - c_u\|^2, \forall u, 1 \leq u \leq k \cap u \neq j \right\} \quad (28)$$

where \$\|X\_i - c\_j\|^2\$ represents the distance between the \$i^{th}\$ sample data and the \$j^{th}\$ cluster center; \$K\_j\$ indicates that the sample \$i\$ belongs to the center \$j\$.

The mean value within each cluster is calculated to obtain new center sample data, and the distance from all data to the center data is recalculated for classification. The algorithm continues to iterate until each cluster center no longer changes.

The RBF network is trained after determining the center parameters of hidden layer by the K-means clustering. Initialize the weights from the hidden layer to the output layer and the width vector corresponding to each central parameter. Then the gradient descent method is used to iteratively train the parameters \$(w, C, D)\$ to determine the proportion of the features represented by each cluster center in the output:

$$\begin{cases} \Delta w_f = \eta \frac{\Delta E}{\Delta w_f} = \eta \sum_{p=1}^N e_p \varphi_f(\|x_p - c_f\|) \\ \Delta c_f = \eta \frac{\Delta E}{\Delta c_f} = \eta \frac{w_f}{d_f^2} \sum_{p=1}^N e_p \varphi_f(\|x_p - c_f\|)(x_p - c_f) \\ \Delta d_f = \eta \frac{\Delta E}{\Delta d_f} = \eta \frac{w_f}{d_f^2} \sum_{p=1}^N e_p \varphi_f(\|x_p - c_f\|) \|x_p - c_f\|^2 \end{cases} \quad (29)$$

where \$\eta\$ is the learning factor; \$E\$ is the evaluation function for RBF neural network, as shown in (30).

$$E = \frac{1}{2} \sum_{g=1}^N e_g^2 = \frac{1}{2} \sum_{g=1}^N (V_{p,g} - Z_g)^2 \quad (30)$$

where \$e\_g\$ is the difference between the network prediction output and the expected output when the \$g^{th}\$ sample data is input; \$N\$ is the number of sample data.

2) *Safety Requirement*: The pursuit of the expected speed is the active intention of human beings, but the requirement of safety is always needed. After obtaining the expected speed from the RBF network, the operation to be performed is judged according to the current environment. If the current traffic environment cannot reach the expected speed, the decision will be rejected and the current state is kept waiting for a suitable time. Whether the expected speed cannot be reached or there is no motivation to change the state, maintaining the existing state may face sudden conditions, such as the sudden sharp deceleration of the preceding vehicle, or the side vehicles arbitrarily merge into the own lane. These may lead to an increase in the risk of maintaining the existing state, and it needs to change the driving state to ensure safety. This is a forced motivation.

When safety is threatened, drivers usually reduce the risk by adjusting longitudinal speed or changing lanes [27], [28].

Therefore, this work combines longitudinal speed adjustment and lateral steering operation. The driving behavior in emergency is divided into: 1) Constant speed lane changing (CLC); 2) Deceleration lane changing (DLC); 3) Braking without lane changing (BA).

The necessary condition for avoiding collision is that the lateral displacement of the autonomous vehicle needs to be larger than the width of the preceding vehicle when they have not collided in the longitudinal direction. A sinusoidal function curve is used to simulate vehicle lane changing:

$$W + \tau = \frac{L_d}{t_e} t_c - \frac{L_d}{2\pi} \sin\left(\frac{2\pi}{t_e} t_c\right) \quad (31)$$

where  $W$  is the width of preceding vehicle;  $\tau$  is the safety margin;  $L_d$  is the width of lane,  $L_d = 3.75$ ;  $t_e$  is the time of lane change,  $t_e = 3.5$ ;  $t_c$  is the critical time to collision.

According to the sensing module, the vehicle width can be obtained, and then  $t_c$  is calculated by solving (31). The minimum distance during CLC and DLC are respectively shown in (32):

$$\begin{aligned} S_c &= (v_e^k - v_f^k)t_c + \frac{1}{2}d_{f,k}t_c^2 \\ S_d &= (v_e^k - v_f^k)t_c - \frac{1}{2}(d_{e\max} - d_{f,k})t_c^2 \end{aligned} \quad (32)$$

where  $v_e^k, v_f^k$  are the speed of autonomous vehicle and preceding vehicle at moment  $k$ ;  $d_{e\max}$  is the maximum deceleration of autonomous vehicle;  $d_{f,k}$  is the deceleration of preceding vehicle at moment  $k$ .

The relative speed has a great influence on whether the driver takes braking or steering to avoid collision. Therefore, the relative speed and the space headway are used as the conversion indicators of the three actions. The probability of three actions taken in an emergency situation are as follows:

$$\begin{cases} P(CL\mid\beta=1) = P(D_0 - S_c > 0\mid\beta=1) \\ \cdot P(v_e - v_f > v_\eta\mid\beta=1) \\ P(DLC\mid\beta=1) = P(S_d < D_0 < S_c\mid\beta=1) \\ \cdot P(v_e - v_f > v_\eta\mid\beta=1) \\ P(BA\mid\beta=1) = P(v_e - v_f < v_\eta\mid\beta=1) \end{cases} \quad (33)$$

where  $D_0$  is the actual distance between the ego vehicle and the preceding vehicle;  $v_\eta$  is the conversion threshold, it can ensure that the vehicle does not take excessive or complex actions when only a slight braking is required;  $\beta$  is the condition parameter to judge whether the emergency situation is triggered or not.

$$\beta = \begin{cases} 1 & \zeta_t^{q,a_0} < \zeta_{safty} \\ 0 & \zeta_t^{q,a_0} > \zeta_{safty} \end{cases} \quad (34)$$

where  $\zeta_t^{q,a_0}$  is the risk when the vehicle is in the lateral position  $q$  and the acceleration is zero.

3) *Destination Needs*: In Fig. 8, the conditions that affect the planning of the local path are not only the subjective psychological pursuit of expected speed and the forced requirement of safety, but also the need of destination (global path). The purpose of local path planning is to split the global path and finally reach the target point. In view of the running condition of highway, the target end point is generally expressed as the off-ramp. The operation behavior is similar to the above behavior

of steering to avoid collision, except that both lanes are available for choice when steering to avoid collision into a fixed lane, and the target point is clear and unchangeable. Therefore, in the following analysis, it is classified as steering avoidance behavior with additional constraints.

### B. Decision Validation Based on Risk Assessment

When making decisions according to the method proposed in Section III-A, there may be a problem that due to the dynamic variability of the traffic environment. When the vehicle maintains the current state or changes the state, only considering the current environment may cause the decision to fail or require adjustment. Therefore, in this paper, the decision results based on motivation are mapped to the risk assessment model constructed in Section II for dynamic environment verification. In this way, the interactivity of driving behavior and the dynamic uncertainty of traffic environment are considered. Meanwhile, the dynamic verification process based on risk assessment is a further improvement of the motivation-based decision and planning method. It can help decision-making methods to determine which behavior can safely achieve the expected speed or which side of the lane is safe when avoiding risks by looking for the optimal target point. If a safe solution cannot be found, it proves that the decision cannot be implemented and needs to be re-decided.

Feature extraction is carried out for the decision result based on motivation. Multiple target points generated by each decision behavior are combined with the risk of the surrounding environment and driving rules and habits. Then, the optimal point under the safety value of risk assessment is selected. The behaviors generated by the above motivation-based decisions can be represented by different acceleration and lateral position sequences:

$$\begin{aligned} A_{t+N_p}^\pi &= [a_\pi(t+N_p, 1), a_\pi(t+N_p, 2), \dots, a_\pi(t+N_p, C_p)]^T \\ Q_{t+N_p}^\pi &= [q_\pi(t+N_p, 1), q_\pi(t+N_p, 2), \dots, q_\pi(t+N_p, C_p)]^T \end{aligned} \quad (35)$$

where  $A_{t+N_p}^\pi, Q_{t+N_p}^\pi$  are the sequence of acceleration and lateral position;  $\pi$  represents different decision motivations;  $C_p$  is the number of candidate points in (22).

On the basis of the candidate sequence of acceleration and lateral position, the objective function is established to find the target point, which should suit for the current traffic environment and can give consideration to both safety and efficiency.

$$\begin{cases} U_a^i(t) = \beta H_{a,\varpi}^i(t) + \lambda G_a^i(t) \\ U_q^j(t) = \beta H_{q,\varpi}^j(t) + \lambda G_q^j(t) \end{cases} \quad (36)$$

where  $H, G$  are the vectors corresponding to the motivations based on safety requirement and expected speed, and their specific expressions are in (37)–(39);  $a, q$  are acceleration and lateral position;  $i, j$  are the number of candidate accelerations and lateral positions;  $\varpi$  is decision-making behavior resulting from security requirements;  $\beta, \lambda$  are weight factors,  $\beta + \lambda = 1$ .

$$H_{a,\varpi}^i = \begin{cases} \frac{C_p(a_0 - a_{\min})}{a_{\max} - a_{\min}} i & P(BA\mid\beta=1) = 1 \\ \frac{2(D_0 - S_2)}{t_c^2} - a_{\min} & P(DLC\mid\beta=1) = 1 \\ a_0 & P(CLC\mid\beta=1) = 1 \end{cases} \quad (37)$$

where  $D_0$  is the actual distance between the ego vehicle and the preceding vehicle;  $a_0$  is the state with zero acceleration.

$$H_{q,\varpi}^j = \begin{cases} q_0 \pm L_d P(CLC|\beta = 1) = 1 \cup P(DLC|\beta = 1) = 1 \\ q_0 \quad P(BA|\beta = 1) = 1 \end{cases} \quad (38)$$

where  $q_0$  is the centerline of the lane where the vehicle is located in.

$$\begin{cases} G_a^i = a_0 + \frac{(a_{\max} - a_{\min})(v_{p,i} - v_{e,\min}^T)}{v_{e,\max}^T - v_{e,\min}^T} \\ G_q^j = l_{\min} + (\Delta l/C_p)j \end{cases} \quad (39)$$

where  $v_{e,\max}^T, v_{e,\min}^T$  are the maximum and minimum speed that the vehicle can reach after a period of time  $T$ .

According to the risk and driving rules, the evaluation function is established to screen the candidate sequences and select the optimal point:

$$J =$$

$$\arg \max \left\{ \frac{N(a - a_0)(q - q_e) + \ell}{M \| (U_a^i, U_q^j) - (a_0, q_e) \|_2 } \mid \zeta(U_a^i, U_q^j) < \zeta_{safety} + \kappa \right\} \quad (40)$$

where  $\| (U_a^i, U_q^j) - (a_0, q_e) \|_2$  indicates the distance between the candidate state of the vehicle and the current state;  $N, M$  are weight factors, and  $M < N$ ;  $\zeta(U_a^i, U_q^j) < \zeta_{safety} + \kappa$  is a prerequisite to exclude candidate points that do not meet the risk threshold to ensure safety;  $\ell$  and  $\kappa$  are extremely small positive and negative numbers.

With the evaluation function, the feedback of each candidate points can be compared to get the optimal point. Then use it as the target end point of local path planning, and lay the foundation for the path and speed planning in Section III-C.

### C. Path-Speed Planning Based on Optimal Point

Generally speaking, with the initial state and target position, a smooth trajectory with quadratic derivability can be planned by using quintic polynomial. However, the trajectory planned by this method is fixed, so the path geometry cannot be adjusted according to the surrounding environment and it has poor flexibility. This work hopes to discretize the trajectory into multiple nodes between the initial state and the target end point, and each node can move within an appropriate range according to the surrounding environment and obtain an optimized optimal trajectory. Obviously, it is difficult to calculate how much each node moves in which direction by what criteria. What's more, the smoothness between the two nodes cannot be guaranteed. Therefore, the action planning method based on Frenet coordinate system is used in this paper to optimize the trajectory and simplify the decision problem into a selection problem.

Unlike the Cartesian coordinate, the Frenet coordinate uses the road center line as the reference line. The direction along the reference line is called the vertical direction ( $s$ ), and the direction perpendicular to the reference line is the horizontal direction ( $d$ ) as shown in Fig. 10. The conversion relationship between Frenet coordinate system and Cartesian coordinate system is

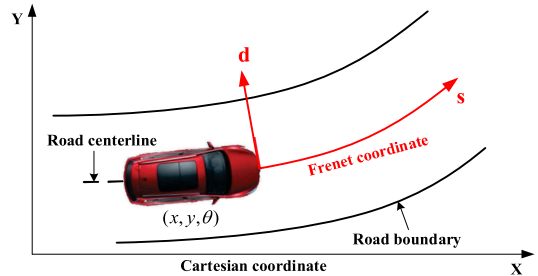


Fig. 10. Frenet coordinate.

referred the literature [29]. It can decouple the two-dimensional motion problem of the vehicle into two one-dimensional motion problems by using the Frenet coordinate system. The direction  $s$  can distribute a reasonable speed to the trajectory, and the direction  $d$  determines the geometry of the trajectory.

1) *Planning of Lateral Trajectory*: When planning a trajectory, the status of the preceding vehicle in the current lane and the vehicle behind the autonomous vehicle in the target lane is the main consideration. For example, in the lane changing process and when the collision risk of the preceding vehicle is higher than that of the side-rear vehicle, the speed change of the desired trajectory in the direction  $s$  is slow first and then rapid, while in the direction  $d$  is opposite. Thus, the vehicle can reach the target lane as soon as possible and avoid collision with the preceding vehicle.

The interval between the initial state  $D_s$  and the final state  $D_e$  is divided into several target end points  $D_t$ . Moreover, the planning period  $T$  is divided into three nodes  $[t_1, t_2, t_3]$ . A candidate trajectory from  $D_s$  to the  $p^{th}$  target endpoint  $D_e$  is planned by using a quintic polynomial:

$$d(t) = a_{d_0} + a_{d_1}t + a_{d_2}t^2 + a_{d_3}t^3 + a_{d_4}t^4 + a_{d_5}t^5 \quad (41)$$

The coefficients of the quintic polynomial are calculated by the constraints between the initial state  $D_s = [d_s, \dot{d}_s, \ddot{d}_s]$  and the target state  $D_t = [d_t, \dot{d}_t, \ddot{d}_t]$ .

$$[d_s, \dot{d}_s, \ddot{d}_s, T] \Rightarrow [d_{t,p}, 0, 0, T] \quad (42)$$

$$\begin{cases} a_{d_0} = d_s \\ a_{d_1} = \dot{d}_s \\ a_{d_2} = \ddot{d}_s / 2 \end{cases} \quad (43)$$

$$\begin{bmatrix} T^3 & T^4 & T^5 \\ 3T^2 & 4T^3 & 5T^4 \\ 6T & 12T^2 & 20T^3 \end{bmatrix} \times \begin{bmatrix} a_{d_3} \\ a_{d_4} \\ a_{d_5} \end{bmatrix} = \begin{bmatrix} d_{t,p} - (d_s + \dot{d}_s T + 0.5\ddot{d}_s T^2) \\ \dot{d}_{t,p} - (\dot{d}_s + \ddot{d}_s T) \\ \ddot{d}_{t,p} - \ddot{d}_s \end{bmatrix} \quad (44)$$

After obtaining multiple sets of candidate trajectories, the cost function is used to filter the trajectories. Then the trajectory with the smallest cost value is selected as the optimal trajectory during  $t_0-t_1$ .

$$\begin{aligned} d_s &= d_{t_1,op}, \dot{d}_s = \dot{d}_{t_1,op}, \ddot{d}_s = \ddot{d}_{t_1,op}, T = T - t_1 \\ &\Rightarrow [d_{t,p}, 0, 0, T - t_1 | d_{t,p} > d_{t_1,op}] \end{aligned} \quad (45)$$

The re-planning of each node is an adjustment and optimization of the trajectory. Meanwhile the new initial state is consistent with the velocity and acceleration of the last state, which also ensures the smoothness of the trajectory. Therefore, the optimization of the entire trajectory is simplified to the selection of each node.

The ability to adjust the trajectory depends on the parameters contained in the cost function and the corresponding weights of each parameter. The cost function must consider the smoothness of the trajectory and finally reach the target state.

$$\begin{cases} C_{d,p} = K_J J_d + K_T T + K_d(d_s - d_e)^2 + K_\xi \dot{d}_s & \xi_f > \xi_r \\ C_{d,p} = K_J J_d + K_T T + K_d(d_s - d_e)^2 + K_\xi / \dot{d}_s & \xi_f < \xi_r \end{cases} \quad (46)$$

where  $J_d$  is the lateral acceleration,  $J_d = \ddot{d}(t)$ , the cost function penalizes the candidate trajectory with large  $J_d$  to ensure that the geometric characteristics of the trajectory change smoothly;  $(d_s - d_e)^2$  indicates the distance to the target state;  $\xi_f, \xi_r$  are the collision risk of the preceding vehicle and the side rear vehicle;  $K_J, K_T, K_d, K_\xi$  are weight factors.  $K_J$  and  $K_T$  are constants.

$K_d$  is a function of time, which increases with the time to ensure that the trajectory finally reaches the target state.  $K_\xi$  is affected by collision risk and time. It is determined by the difference between  $\xi_f$  and  $\xi_r$  when adjusting the geometry of the trajectory is the main target. As time goes on, the main goal changes to reach the target point and  $K_\xi$  keeps decreasing.

$$K_d = k_d \exp(t) \quad (47)$$

$$K_\xi = k_\xi \exp(|\xi_f - \xi_r|/t) \quad (48)$$

where  $k_d$  and  $k_\xi$  are the initial constant value;  $t \in [t_1, t_2, t_3]$ .

2) *Planning of Speed*: After determining the geometry of trajectory in direction  $d$ , the velocity is allocated in direction  $s$ . This part takes the expected speed as the target point which is obtained in Section III-B.

The planning process of velocity is similar to the planning process of lateral trajectory, but the target state and the polynomial coefficient solution matrix are changed.

$$[S_s, \dot{S}_s, \ddot{S}_s, T] \Rightarrow [\dot{S}_e, \ddot{S}_e = 0, \ddot{\ddot{S}}_e = 0, T] \quad (49)$$

$$\begin{cases} a_{s0} = s_s \\ a_{s1} = \dot{s}_s \\ a_{s2} = \ddot{s}_s/2 \\ a_{s3} = \ddot{\ddot{s}}_s/6 \end{cases} \quad (50)$$

$$\begin{bmatrix} 4T^3 & 5T^4 \\ 12T^2 & 20T^3 \end{bmatrix} \times \begin{bmatrix} a_{s4} \\ a_{s5} \end{bmatrix} = \begin{bmatrix} \dot{s}_e - (\dot{s}_s + \ddot{s}_s T + 0.5 \ddot{\ddot{s}}_s T^2) \\ \ddot{s}_e - (\ddot{s}_s + \ddot{\ddot{s}}_s T) \end{bmatrix} \quad (51)$$

where  $S_s$  and  $S_e$  are the initial state and the final state.

The cost function is changed to punish the candidate set far away from the expected speed, and the longitudinal acceleration is adjusted according to the risk of collision.

$$\begin{cases} C_{s,p} = K_J J_s + K_T T + K_d(\dot{s}_s - \dot{s}_e)^2 + K_\xi / \ddot{s}_s & \xi_f > \xi_r \\ C_{s,p} = K_J J_s + K_T T + K_d(\dot{s}_s - \dot{s}_e)^2 + K_\xi \ddot{s}_s & \xi_f < \xi_r \end{cases} \quad (52)$$

Fig. 11 shows the results of path-speed simulation planning. The trajectories A and B represent two cases of  $\xi_f > \xi_r$  and

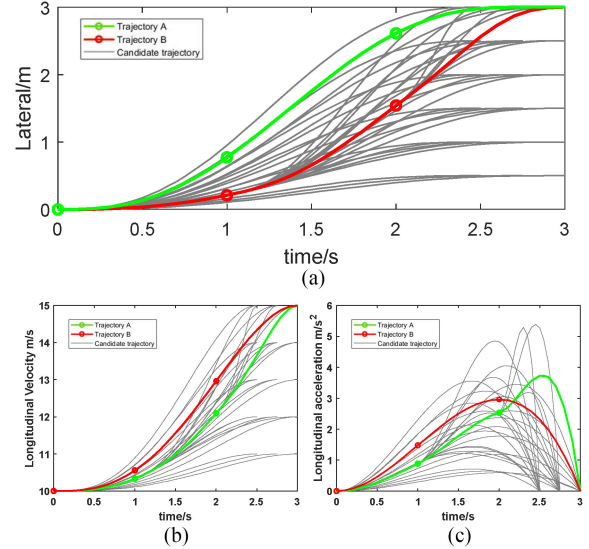


Fig. 11. The result of path-speed planning. (a) Lateral trajectory under different scenarios. (b) Speed distribution under different scenarios. (c) Acceleration distribution under different scenarios.

$\xi_f < \xi_r$  respectively, and the gray curves represent the candidate trajectories. The layering of the candidate set in the lateral direction of Fig. 11(a) and (b) corresponds to the transition state between the initial and final states, which indicate the process of the lateral position and speed approaching to the target value. Taking the trajectory A in Fig. 11 as an example, it indicates that when the collision risk of preceding vehicle is high, the lateral trajectory will turn to the target lane as early as possible. The speed will change little at the initial stage and then accelerate more after entering the target lane. Meanwhile, the peak value of acceleration also appears later in Fig. 11(c). When the collision risk of side-rear vehicle is high, the characteristics of the lateral trajectory and speed distribution are just the opposite. Therefore, the path and speed planning method proposed in this paper can be a good way to adjust the path and speed flexibly according to different environments.

#### IV. SIMULATION RESULTS

The required parameters and training data of the probability prediction model and the motivation model based on the RBF network are extracted through the NGSIM database, and then the prediction results of the above models are verified. Moreover, in order to verify and demonstrate the effectiveness of the proposed decision method in Section III, driving simulations are carried out for three scenarios: normal driving, cut-in and road construction, where multiple surrounding vehicles are driving on a three-lane highway. The main simulation parameters are shown in Table II.

##### A. Data Extraction and Analysis

The NGSIM database is widely used for the calibration and validation of existing traffic simulation models. There are four datasets in the NGSIM database and the dataset of US-101 is most widely used to verify models. Note that this dataset is

TABLE II  
SIMULATION PARAMETERS

Parameter	Description	Value(units)
$L_d$	Lane width	3.75m
$n$	Number of lanes	3
$a_{ran}$	Acceleration range of ego vehicle	[-4, 3]
$T$	Time domain for predicting and planning	3s
$\xi_{safy}$	Safety risk threshold	33
$\gamma$	Time loss factor	0.8
$d_{set}$	Initial reference position of lateral trajectory	5.25m

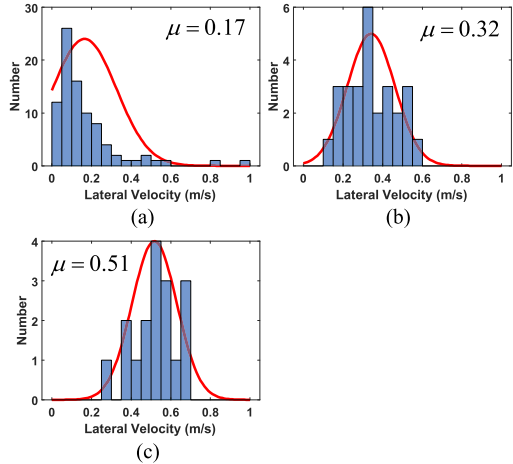


Fig. 12. Relationship between lateral speed and driving behavior. (a) Lateral speed distribution of lane keeping. (b) Lateral speed distribution of lane changing. (c) Lateral speed distribution of double lane changing.

collected on a straight highway with approximately 500 meters in length and consisted of one on-ramp and six freeway lanes.

In Section II, the surrounding vehicle probability prediction model is built. The MTPM based on the lateral velocity is used to find the probability of the target lane transition. The MTPM is established based on the lateral velocity distribution of lane keeping, lane changing and double lane changing. The lateral velocity distributions of different behaviors are extracted from the NGSIM database. Fig. 12 shows the relationship between lateral speed and driving behavior. Each driving behavior satisfies the Gaussian distribution, which corresponds to different mean values as shown in (53).

$$\begin{cases} \text{for } |i - j| = 0; \quad \mu_0 = \text{sgn}(i - j) \cdot 0.17; \quad \sigma_0 = 0.08 \\ \text{for } |i - j| = 1; \quad \mu_1 = \text{sgn}(i - j) \cdot 0.32; \quad \sigma_1 = 0.17 \\ \text{for } |i - j| = 2; \quad \mu_2 = \text{sgn}(i - j) \cdot 0.51; \quad \sigma_2 = 0.20 \end{cases} \quad (53)$$

The initial transition probability matrix and the initial probability distribution are defined as (54).

$$T_{ij}^{ini}(\dot{q}) = \begin{bmatrix} 0.60 & 0.39 & 0.01 \\ 0.20 & 0.60 & 0.20 \\ 0.01 & 0.39 & 0.60 \end{bmatrix} \quad (54)$$

$$X_t^i = [1/3; 1/3; 1/3;]^T \quad (55)$$

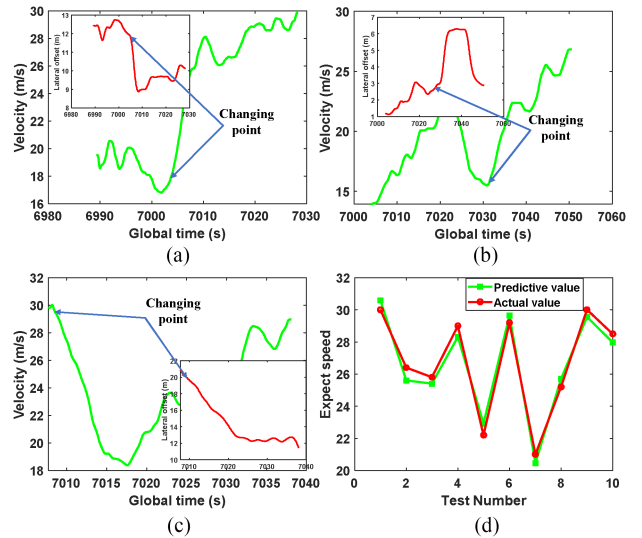


Fig. 13. Training set extraction and result verification of RBF network. (a)–(c) Relationship between path and speed when the driving state changes. (d) Prediction result of RBF network.

Fig. 13 shows the training set extraction and result verification of RBF network. The behavior characteristics of the typical driver are extracted in the US-101 dataset when the driving state is changing. The green curve represents the speed, and the red curve represents the path. Then, the relevant conditional factors are as the training sample of the RBF network. Moreover, the actual driver information in the database is used to verify the trained RBF network, and the accuracy of the network prediction is verified in Fig. 13(d). Note that the test sample as verification is independent of the training sample

### B. Cases Study

Fig. 14 to Fig. 16 are the simulation results, and mainly include: (a) Road scene, ①, ②, ③ are lane sequence; (b) Predicted trajectories of surrounding vehicles, and the  $ds$  axis represents the relative displacement in the predicted time domain  $T$ ; (c) The collision risk map of the ego vehicle under different accelerations in different lanes and the optimal point obtained by the decision method, where the interval of ordinate corresponds to the lane sequence in part (a) (d) Path-speed planning results based on the optimal point, d-1, d-2, d-3, d-4 are the lateral position, longitudinal position, speed and acceleration respectively.

1) *Normal Driving Scenario*: As shown in Fig. 14(a), the first scene is that the ego vehicle is driving normally in lane ② with the speed of 25 m/s, and there is a vehicle A in front of the ego vehicle with the speed of 20 m/s. Considering that there is a large relative speed between the two vehicles, the ego vehicle attempts to change the current state to ensure the expected speed. Note that the vehicle B in the lane ① does not have a tendency to accelerate. It can be seen from the environmental risk assessment map of the ego vehicle in Fig. 14(c) that the risk of the lane ① is lower than the safety threshold. Therefore, based on the motivational decision-making method, the RBF network determines the expected speed according to the current environmental state,

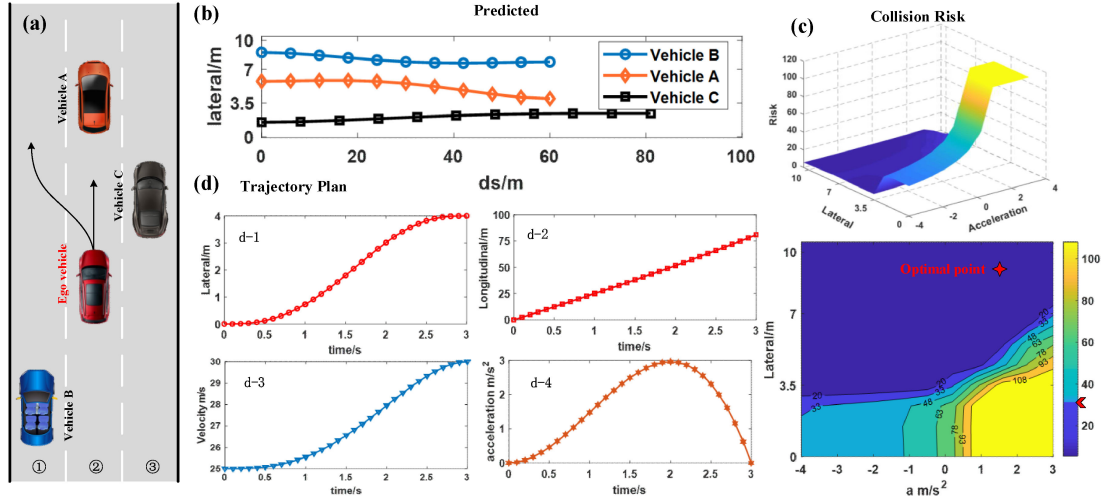


Fig. 14. Simulation result of normal driving scenario. (a) Road scene. (b) Predicted trajectories of surrounding vehicles. (c) Collision risk map. (d) Path-speed planning result.

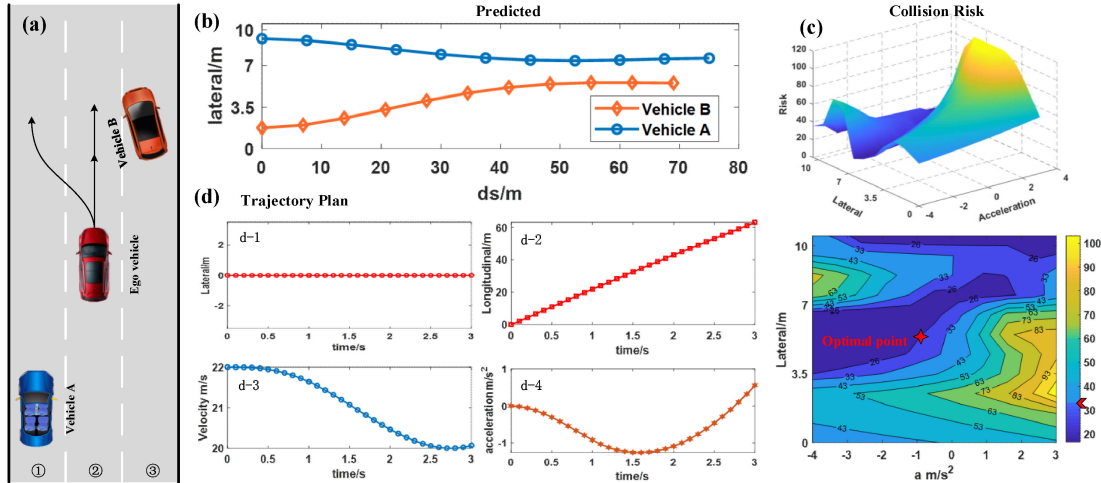


Fig. 15. Simulation result of cut in scenario. (a) Road scene. (b) Predicted trajectories of surrounding vehicles. (c) Collision risk map. (d) Path-speed planning result.

and the decision result is to take an accelerated lane change to lane ①, thereby ensuring the driving efficiency. The changing process of speed and acceleration are presented in Fig. 14(d-3), (d-4), and the expected speed is 30 m/s.

2) *Cut in Scenario:* As shown in Fig. 15(a), in the second scenario, the ego vehicle is driving normally in lane ② at a speed of 22 m/s. There is no vehicle ahead and the speed of ego vehicle is lower than the road limit speed. The prediction model predicts that vehicle B is about to change lanes to the front of ego vehicle in Fig. 15(b), and its speed is 20 m/s. Since the cut-in position of vehicle B is closer to ego vehicle, ego vehicle has to change the driving state. According to the risk assessment map in Fig. 15(c), ego vehicle can take left lane change or deceleration to reduce the risk. Note that vehicle A is accelerating, while the relative speed of vehicle B and ego vehicle is small. Therefore, it is optimal to take appropriate deceleration to reduce the risk, and the planning result is presented in Fig. 15(d).

3) *Road Construction Scenario:* As shown in Fig. 16(a), in the third scenario, the ego vehicle is following the vehicle A and normally driving on the lane ② at a speed of 25 m/s. At a certain moment, vehicle A finds that there is an obstacle in front and changes lane to lane ③. At the next moment, ego vehicle senses the obstacle at a distance of 80 m ahead and needs to take action to avoid a collision accident. There is a large relative speed between ego vehicle and the obstacle, and the space headway of the ego vehicle is greater than the safe distance  $S_c$  required by the driving behavior CLC. Meanwhile, the risk assessment map shows that the risk value for the state of lane ③ and zero acceleration is under the safety threshold. Therefore, ego vehicle drives towards to lane ③ following the vehicle A.

From the simulation results of the above three scenarios, it can be seen that the path, speed and acceleration sequence calculated by the decision-making and planning algorithm based on motivation and risk assessment are continuous and smooth, which meets the vehicle kinematics constraints and control

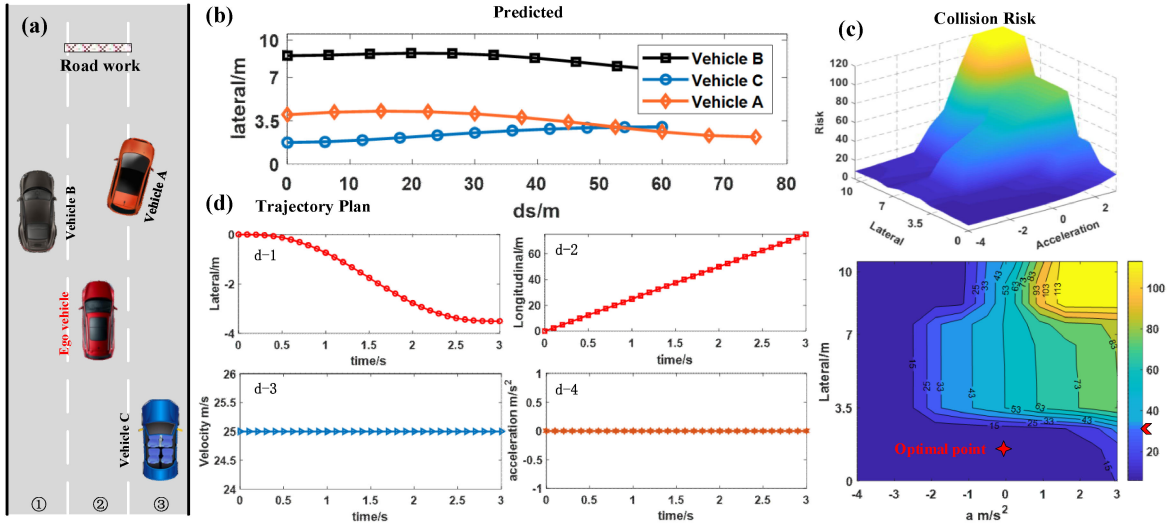


Fig. 16. Simulation result of road construction scenario. (a) Road scene. (b) Predicted trajectories of surrounding vehicles. (c) Collision risk map. (d) Path-speed planning result.

TABLE III  
RUNNING TIME OF EACH MODULE

Module	Prediction	Risk Assessment	Decision Process	Planning
Average Time	0.042s	0.009s	0.128s	0.35s

requirements. In addition, in both the normal driving scenario and the cut-in scenario, there is an interfering car on the left rear of the ego vehicle that may affect the decision. The difference is that the blue vehicle has a tendency to accelerate in cut-in scenario. For the decision result, in Fig. 14, the autonomous vehicle performs lane change while in Fig. 15, the vehicle chooses deceleration and avoidance, which accurately avoid the potential collision risk caused by the acceleration of the blue vehicle. It reflects the flexible adjustment ability of the algorithm proposed in this paper with the change of influencing factors in similar scenarios.

Table III shows the running time of each module of the algorithm proposed in this paper. During the driving process, the risk assessment module runs continuously to ensure safety. It can be seen that it has good real-time performance. The decision-making process includes the whole process of prediction module, motivational decision and dynamic verification based on risk assessment. The average time of the whole decision-making process is 0.1 s to 0.15 s, and the planning module includes two parts: path and speed.

In addition, the method proposed in this paper is compared with the sampling-based rapid search random tree algorithm (RRT) as shown in the Fig. 17. The simulation condition is normal driving scenario which is described in Fig. 14. Due to the randomness of sampling probability, the final trajectory of RRT is often not definite and optimal. Meanwhile, calling the collision detection function for each extended node also

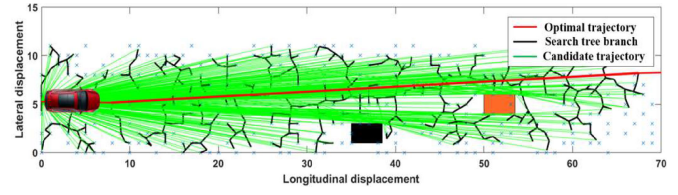


Fig. 17. Simulation results of RRT algorithm.

wastes a lot of time. The entire decision and planning time based on the RRT algorithm is 0.8s-1.2s. We also compared the improved algorithm of RRT (RRT-Connect, B-RRT\*). The average planning time of the two methods is 0.65s and 0.53s respectively. However, under the same working conditions, the decision and planning time of this work is 0.5s. It is worth noting that when the surrounding environment does not change frequently, the algorithm proposed in this work does not need to participate in the calculation every time. Thus, the calculation efficiency has been significantly improved.

## V. CONCLUSION

This work proposes a decision-making and planning method for autonomous vehicles based on motivation and risk assessment. The proposed method firstly analyzes the current driving environment to determine whether there is a motivation to change the driving state or not. The driving behavior is decided and planned when the motivation is triggered. Otherwise, the current state is maintained. Meanwhile, in order to ensure the safety of autonomous vehicles, a risk assessment model of the surrounding environment is established for early warning and decision verification. In addition, the planned trajectory in this paper can flexibly adjust its geometry and speed distribution according to the surrounding environment, which is more in line with actual situation. The simulation results show that the method can determine appropriate driving behavior and plan a

trajectory that meets vehicle dynamic requirements in a complex highway environment.

This article focuses on the analysis of driving motivation under highway conditions. In future research, the urban environments which is more complexed need to be analyzed to make the decision-making process safer, more flexible, and more in line with the requirements of human drivers.

## REFERENCES

- [1] L. Zhao R. Ichise Y. Sasaki Z. Liu and T. Yoshikawa “Fast decision making using ontology-based knowledge base,” in *Proc. IEEE Intell. Veh. Symp.*, Gothenburg, 2016, pp. 173–178.
- [2] M. C. Turan, A. E. Hartavi, and E. Altug, “Development of a rule based upper level control algorithm for a co-operative vehicle in automated highway system,” in *Proc. IEEE Int. Conf. Veh. Electron. Saf.*, Istanbul, 2012, pp. 454–459.
- [3] L. Zhao and R. Ichise, “Fast decision making using ontology-based knowledge base,” in *Proc. IEEE Intell. Veh. Symp.*, Gothenburg, 2016, pp. 173–178.
- [4] D. Lenz, F. Diehl, M. T. Le, and A. Knoll, “Deep neural networks for markovian interactive scene prediction in highway scenarios,” in *Proc. IEEE Intell. Veh. Symp.*, Los Angeles, CA, USA, 2017, pp. 685–692.
- [5] X. Zhou, W. Wang, T. Wang, Y. Lei, and F. Zhong, “Bayesian reinforcement learning for multi-robot decentralized patrolling in uncertain environments,” *IEEE Trans. Veh. Technol.*, vol. 68, no. 12, pp. 11691–11703, Dec. 2019.
- [6] Q. Wang and C. Phillips, “Cooperative collision avoidance for multi-vehicle systems using reinforcement learning,” in *Proc. 18th Int. Conf. Methods Models Automat. Robotics*, 2013, pp. 98–102.
- [7] H. Bai *et al.*, “Intention-aware online POMDP planning for autonomous driving in a crowd,” in *Proc. IEEE Int. Conf. Robot. Auto.*, Seattle, WA, USA, 2015, pp. 454–460.
- [8] A. Zyner, S. Worrall, and E. Nebot, “A recurrent neural network solution for predicting driver intention at unsignalized intersections,” *IEEE Robot. Automat. Let.*, vol. 3, no. 3, pp. 1759–1764, Jul. 2018.
- [9] M. Bahram *et al.*, “A game-theoretic approach to replanning-aware interactive scene prediction and planning,” *IEEE Trans. Veh. Technol.*, vol. 65, no. 6, pp. 3981–3992, Jun. 2016.
- [10] Z. Chen and X. Huang, “End-to-end learning for lane keeping of self-driving cars,” in *Proc. IEEE Intell. Veh. Symp.*, Los Angeles, CA, USA, 2017, pp. 1856–1860.
- [11] D. Isele *et al.*, “Navigating occluded intersections with autonomous vehicles using deep reinforcement learning,” in *Proc. IEEE Int. Conf. Robot. Automat.*, Brisbane, QLD, 2018, pp. 2034–2039.
- [12] A. Furda and L. Vlase, “Enabling safe autonomous driving in real-word city traffic using multiple criteria decision-making,” *IEEE Trans. Intell. Transp. Syst.*, vol. 3, no. 1, pp. 4–17, 2011.
- [13] C. Xu, W. Zhao, and C. Wang, “An integrated threat assessment algorithm for decision-making of autonomous driving vehicles,” *IEEE Trans. Intell. Transp. Syst.*, vol. 21, no. 6, pp. 2510–2521, Jun. 2020.
- [14] R. Daily and D. M. Bevly, “Harmonic potential field path planning for high speed vehicles,” in *Proc. Amer. Control Conf.*, Seattle, WA, USA, 2008, pp. 4609–4614.
- [15] N. Wahid *et al.*, “Study on potential field based motion planning and control for automated vehicle collision avoidance systems,” in *Proc. IEEE Int. Conf. Mechatr.*, 2017, pp. 208–213.
- [16] J. Ji, A. Khajepour, W. W. Melek, and Y. Huang, “Path planning and tracking for vehicle collision avoidance based on model predictive control with multi constraints,” *IEEE Trans. Veh. Technol.*, vol. 66, no. 2, pp. 952–964, Feb. 2017.
- [17] L. Li, K. Ota, and M. Dong, “Humanlike driving: Empirical decision-making system for autonomous vehicles,” *IEEE Trans. Veh. Technol.*, vol. 67, no. 8, pp. 6814–6823, Aug. 2018.
- [18] D. González, J. Pérez, V. Milanés, and F. Nashashibi, “A review of motion planning techniques for automated vehicles,” *IEEE Trans. Intell. Transp. Syst.*, vol. 17, no. 4, pp. 1135–1145, Apr. 2016.
- [19] D. Aarno, D. Kragic, and H. I. Christensen, “Artificial potential biased probabilistic roadmap method,” in *Proc. IEEE Int. Conf. Robot. Automat.*, New Orleans, LA, USA, 2004, vol. 1, pp. 461–466.
- [20] F. Alesiani and C. Wuthishuwong, “Locally growing rapid tree (LGRT) motion planning for autonomous driving,” in *Proc. IEEE 19th Int. Conf. Intell. Transp. Syst.*, 2016, pp. 1120–1125.
- [21] W. Xu, J. Wei, J. Dolan, H. Zhao, and H. Zha, “A real-time motion planner with trajectory optimization for autonomous vehicle,” in *Proc. IEEE Int. Conf. Robot. Auto.*, 2012, vol. 1, pp. 2061–2067.
- [22] J. Kim and D. Kum, “Collision risk assessment algorithm via lane-based probabilistic motion prediction of surrounding vehicles,” *IEEE Trans. Intell. Transp. Syst.*, vol. 19, no. 9, pp. 2965–2976, Sep. 2018.
- [23] P. Liu, A. Kurt, and Ü. Özgüner, “Trajectory prediction of a lane changing vehicle based on driver behavior estimation and classification,” in *Proc. IEEE 17th Int. Conf. Intell. Transp. Syst.*, Qingdao, 2014, pp. 942–947.
- [24] Y. Xing *et al.*, “Driver lane change intention inference for intelligent vehicles: Framework, survey, and challenges,” *IEEE Trans. Veh. Technol.*, vol. 68, no. 5, pp. 4377–4390, May 2019.
- [25] T. Kondoh and T. Yamamura, “Identification of visual cues and quantification of drivers’ perception of proximity risk to the lead vehicle in car-following situations,” *Mech. Systems. Transp. Logist.*, vol. 1, no. 2, pp. 170–180, 2008.
- [26] W. Tseng and S. Liao, “An expert system using RBF neural network for estimating vehicle speed based on length of skid mark,” in *Proc. 7th Int. Conf. Natural Computation*, 2011, pp. 631–635.
- [27] J. Funke *et al.*, “Collision avoidance and stabilization for autonomous vehicles in emergency scenarios,” *IEEE Trans. Contr. Syst. Technol.*, vol. 25, no. 4, pp. 1204–1216, Jul. 2017.
- [28] C. Lin, J. Juang, and K. Li, “Active collision avoidance system for steering control of autonomous vehicles,” *IET Intell. Transp. Syst.*, vol. 8, no. 6, pp. 550–557, Sep. 2014.
- [29] J. Schlechtriemen, K. P. Wabersich, and K. Kuhnert, “Wiggling through complex traffic: Planning trajectories constrained by predictions,” in *Proc. IEEE Intell. Veh. Symp.*, 2016, pp. 1293–1300.



**Yisong Wang** received the B.S. degree in vehicle engineering from the Nanjing University of Aeronautics and Astronautics, Nanjing, China, in 2019. He is currently working toward the M.S. degree with the Department of Vehicle Engineering, Nanjing University of Aeronautics and Astronautics, Nanjing. His research interests include decision making, trajectory planning and motion control of intelligent vehicle.



**Chunyan Wang** received the B.S. and Ph.D. degrees in mechanical engineering from Jilin University, Changchun, China, in 2000 and 2008, respectively. She is currently a Professor with the Department of Vehicle Engineering, Nanjing University of Aeronautics and Astronautics, Nanjing, China. Her research interests include intelligent vehicle and vehicle system dynamics.



**Wanzhong Zhao** received the B.S. and M.S. degrees in vehicle engineering from Jiangsu University, Zhenjiang, China, in 2004 and 2005, respectively, and Ph.D. degree in vehicle engineering from the Beijing Institute of Technology, Beijing, China, in 2009. He is currently a Professor and the Director with the Department of Vehicle Engineering, Nanjing University of Aeronautics and Astronautics, Nanjing, China. His research interests include intelligent vehicle and vehicle system dynamics.



**Can Xu** received the B.S. degree in agricultural mechanization engineering from Nanjing Agricultural University, Nanjing, China, in 2017. He is currently the Ph.D. candidate with the Department of Vehicle Engineering, Nanjing University of Aeronautics and Astronautics, Nanjing, China. His research interests include decision-making and control of intelligent vehicle.